ADVANCED FUNCTIONAL MATERIALS
www.afm-journal.de

Functional Organic Semiconductors Assembled via Natural Aggregating Peptides

*Galen L. Eakins, Rishi Pandey, Jonathan P. Wojciechowski, Han Yue Zheng, James E. A. Webb, Céline Valéry, Pall Thordarson, Natalie O. V. Plank, Juliet A. Gerrard, and Justin M. Hodgkiss**

Specific peptide sequences designed by inspection of protein–protein interfaces have been identified and used as tectons in hybrid functional materials. Here, an 8-mer peptide derived from an interface of the peroxiredoxin family of self-assembling proteins is exploited to encode the assembly of the perylene imide-based organic semiconductor building blocks. By augmenting the peptide with additional functionality to trigger aggregation and manipulate the directionality of peptide-semiconductor coupling, a series of hybrid materials based on the natural peptide interface is presented. Using spectroscopic probes, the mode of self-assembly and the electronic coupling between neighboring perylene units is shown to be strongly affected by the number of peptides attached, and by their backbone directionality. The disubstituted material with peptides extending in the N to C direction away from the perylene core exhibits strong coupling and long-range order, both attractive properties for electronic device applications. A bio-organic field-effect transistor is fabricated using this material, highlighting the possibilities of exploiting natural peptide tectons to encode self-assembly in other functional materials and devices.

1. Introduction

The emergence of complex molecular assemblies in natural biological systems highlights the potential of using proteins and peptides to rationally encode the assembly of functional synthetic structures in water.[1–3] For example, while the peroxiredoxin (Prx) family of proteins principally exists as obligate homodimers that further self-assemble into toroidal oligomers,[4] some Prx proteins can be induced to form other supramolecular assemblies[5] such as toroidal stacks,[6,7] tubes,[4,8] clusters,[9] and cages.[10] Identifying the native binding interfaces opens the possibility of exploiting them as building blocks in hybrid materials. Such materials may then be used in devices with entirely different functionalities from their parent proteins. Here, we advance this idea by augmenting organic semiconductor materials with peptides identified from Prx proteins to create organic semiconductor assemblies and transistor devices.

Central to the Prx architectures is the antiparallel β-continuous interface that enables the noncovalent dimerization of two protein units via the same β-strand of each. Isolation of the β-strand peptides (typically a seven to eight amino acid sequence) out of such interfaces from a variety of protein types has been shown to yield sequences which show liquid crystallinity and which intrinsically self-assemble into nanoarchitectures while also retaining some properties of their parent protein interfaces.[11] Thus, peptides collected from these types of naturally optimized protein interfaces[12,13] are excellent candidates as tectons for synthetic self-assembly.[11]

While natural peptide interfaces have yet to be exploited in electronic devices, a number of related studies using natural materials highlight the potential of this approach to create new properties and applications.[14] For example, peptides,[15] natural proteins,[16] and DNA-based biopolymers derived from meat processing waste[17] have been used as insulating gate dielectric layers in field-effect transistors. Peptides, proteins, and DNA have also been explored as the active layer components of transistor devices;[18–21] however, this approach is hindered by the wide bandgap and low conductivity of the naturally available electroactive units. Coupling peptides to synthetic organic semiconductors offers a more promising avenue to exploit

G. L. Eakins, H. Y. Zheng, Dr. N. O. V. Plank, Dr. J. M. Hodgkiss
MacDiarmid Institute for Advanced Materials and Nanotechnology
School of Chemical and Physical Sciences
Victoria University of Wellington
P.O. Box 600, Wellington, 6140, New Zealand
E-mail: Justin.Hodgkiss@vuw.ac.nz

R. Pandey
Biomolecular Interaction Centre
University of Canterbury
Private Bag 4800, Christchurch 8140, New Zealand

J. P. Wojciechowski, Dr. J. E. A. Webb, Prof. P. Thordarson
School of Chemistry, the Australian Centre for Nanomedicine and the ARC Centre of Excellence for Convergent Bio-Nano Science and Technology
The University of New South Wales
Sydney, NSW 2052, Australia

Dr. C. Valéry
School of Medical Sciences
RMIT University
P.O. Box 71, Bundoora, VIC 3083, Australia

Prof. J. A. Gerrard
MacDiarmid Institute for Advanced Materials and Nanotechnology
School of Biological Sciences and School of Chemical Sciences
University of Auckland
Thomas Building (Research)
Building 110, 3a Symonds Street, Auckland Central 1010, New Zealand

DOI: 10.1002/adfm.201502255

peptide assembly in the conductive components of electronic devices.[22–24] Non-natural peptides have been used to control the assembly of synthetic molecular semiconductors[25–28] and have been shown to enhance charge mobilities in organic photovoltaic and field-effect transistor devices.[29]

Herein, we present a new family of bioelectronic materials featuring the semiconducting molecule perylene diimide (PDI) coupled to derivatives of the natural self-assembling peptide identified in the bovine Prx3 protein. The β-continuous interface is retained in the hybrid material upon triggered aggregation of nanofibers. The electronic coupling between neighboring PDIs is profoundly affected by the peptide tecton, as revealed by optical spectroscopy. These new properties are exploited through fabricating a water-processed bio-organic field-effect transistor (biOFET) based on a native β-interface.

2. Results and Discussion

2.1. Material Design

Scheme 1A illustrates the natural self-assembly of the Prx3 protein via a β-continuous interface with the IKHLSVN sequence. Before attempting to synthesize this sequence and couple it to PDIs (Scheme 1B), the synthetic route must be carefully considered. Standard solid-phase peptide synthesis (SPPS) protocols are used to access the 7-mer peptide[28,30] and after cleaving from the resin, the peptide amine groups are condensed with perylene anhydride precursors in molten imidazole.[28,31] Accordingly, the native IKHLSVN sequence presented the possibility of amine condensation reactions at both the peptide amino terminus and on the lysine side chain. While perylene imides formed exclusively with the lysine side chain were initially synthesized as test compounds (see the Supporting Information Compounds S1 and S2), coupling through the peptide amine terminus was of primary interest since it would not disrupt the β-interface. This issue was addressed via two alternate strategies. The lysine residue of the original IKHLSVN sequence could either be protected until after forming the imide, or it could be replaced with arginine to permit the terminal coupling mode depicted in Scheme 1B (i.e., IRHLSVN). Based on residue substitution matrices, which assess the probability of a given amino acid substitution in natural systems,[32,33] arginine was expected to be a favorable natural mutation and synthetically advantageous. While acting as a favorable natural replacement preserving the charged character of the lysine position in the peptide sequence, arginine also afforded the advantage of being inert toward the amine condensation reaction.

The primary aggregating IRHLSVN sequence was further augmented at either end with groups to control its hybridization with perylene and to manipulate the hybrid material, as shown in **Scheme 2**A. The opposite end to where the perylene imide core is to be coupled featured three glutamic acid residues. These ionizable residues assisted with solubility of the final peptide–perylene imide product and also provided a means to invoke pH-triggered self-assembly in the compounds.[25,27,28,34,35] At the other end, a two-carbon linking unit with a reactive amino moiety was added to provide a low steric

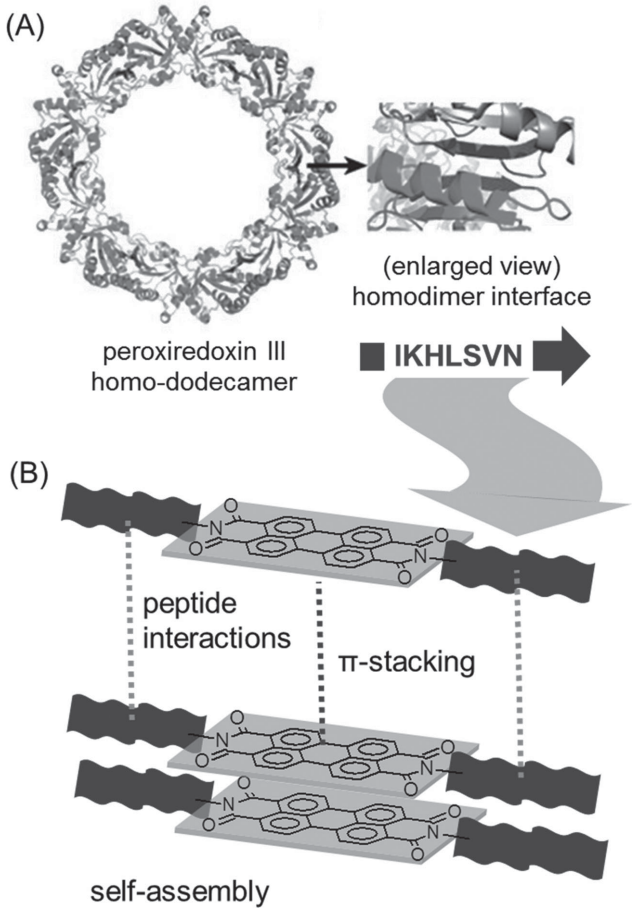

Scheme 1. A) Protein homo-oligomer (pdb crystal structure for peroxiredoxin III (Prx3) homo-dodecamer (1ZYE) with enlarged view into the homodimer IKHLSVN peptide interface (interface contacts shown in red (dark arrows), as determined by PISA software). B) Incorporation of a modified IKHLSVN interface peptide into a perylene diimide, yielding organic semiconductor nanofiber self-assembly from perylene core π-stacking directed by interface peptide β-sheet formation.

demand spacer unit between the perylene core and the central binding region of the peptide.

Using this three-region strategy, two versions of the peptide moiety were synthesized in order to permit two modes of attachment to the perylene imide core and investigate how the peptide assembly influenced the electronic properties of the core. In the "forward-attached" case, the peptide was attached via the amino terminus using a glycine linker such that peptide backbone extends away from the core with an N to C orientation. In the "reverse-attached" case, the peptide was attached via the carboxyl terminus using an ethylamino linker, allowing reversal of the peptide backbone orientation to C to N extending away from the core. This did not simply represent the reversal of residue sequence order relative to the core (which would conserve the N to C peptide backbone orientation relative to the perylene imide core); rather, as shown in Scheme 2, this design produced compound pairs in which the same central binding sequence is attached in each compound within the pair by opposite ends of its backbone with the —Glu—Glu—Glu region always positioned distal to the perylene imide core.

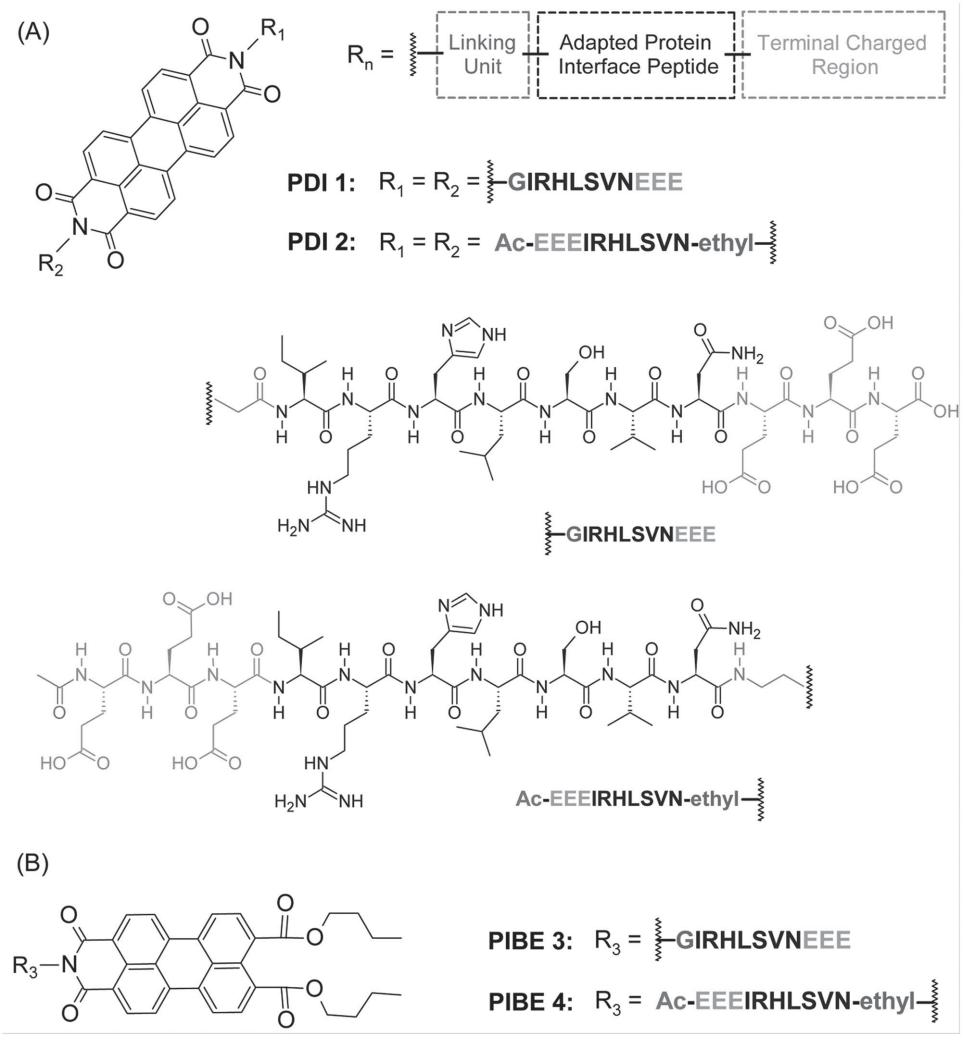

Scheme 2. Structures of the compounds investigated in this study, employing adaptations of the Prx3 homo-dodecamer protein interface peptide: A) dipeptide-PDIs and B) peptide-PIBEs.

Additionally, for the forward- and reverse-attached peptide modes, two different perylene imide core variations were examined for self-assembly using the adapted Prx3 interface. Compounds **1** and **2** represented a complementary pair of symmetrically disubstituted PDIs, while compounds **3** and **4** provided an analogous pair of perylene imide bisesters (PIBEs) each substituted with a single-peptide substituent.

2.2. Aggregation in Peptide–Perylene Imide Conjugates

Since the peptide sequences to be coupled with perylene imides were adaptations of the original Prx3 peptide, synthetic peptides lacking the perylene imide were first compared with the original peptide. Several complementary experiments confirmed that the adapted peptides retained the strong β-sheet forming behavior of the original sequence after the modifications. Spectral features indicative of β-sheets are characterized in the UV range of circular dichroism (CD) spectra via a spectral profile with a positive band maximum near 190–200 nm followed by a single, often broad, and trailing negative band with a minimum near 215–220 nm.[36] Consistent with this profile, **Figure 1**A shows that each of the peptide mutants retains the same CD spectral shape that characterizes β-sheets in the native sequence. The formation of β-sheets was further verified via a thioflavin-T (ThT) fluorescence assay of the peptide mutations (Figure 1B). When this fluorophore binds to β-sheets, its excitation and emission maxima shift from 385 and 445 nm to 450 and 485 nm, enabling simple quantification of the extent of β-sheet assembly,[37,38] which is what was observed when ThT was blended with the native and mutant peptide sequences investigated here. These observations were found to be in agreement with analysis of the amide I band of the IR spectra[39–42] for the targeted GIRHLSVNEEE and Ac-EEEIRHLSVN-ethylamine sequences (see Supporting Information Figures S25 and S26), which displayed a band near 1630 cm^{-1} indicative of β-sheet structures. The β-sheet interactions expressed by the native peptide variants were additionally found to produce ordered peptide nanostructures as observed via transmission electron microscopy (TEM; Figure 1C–F). The results in

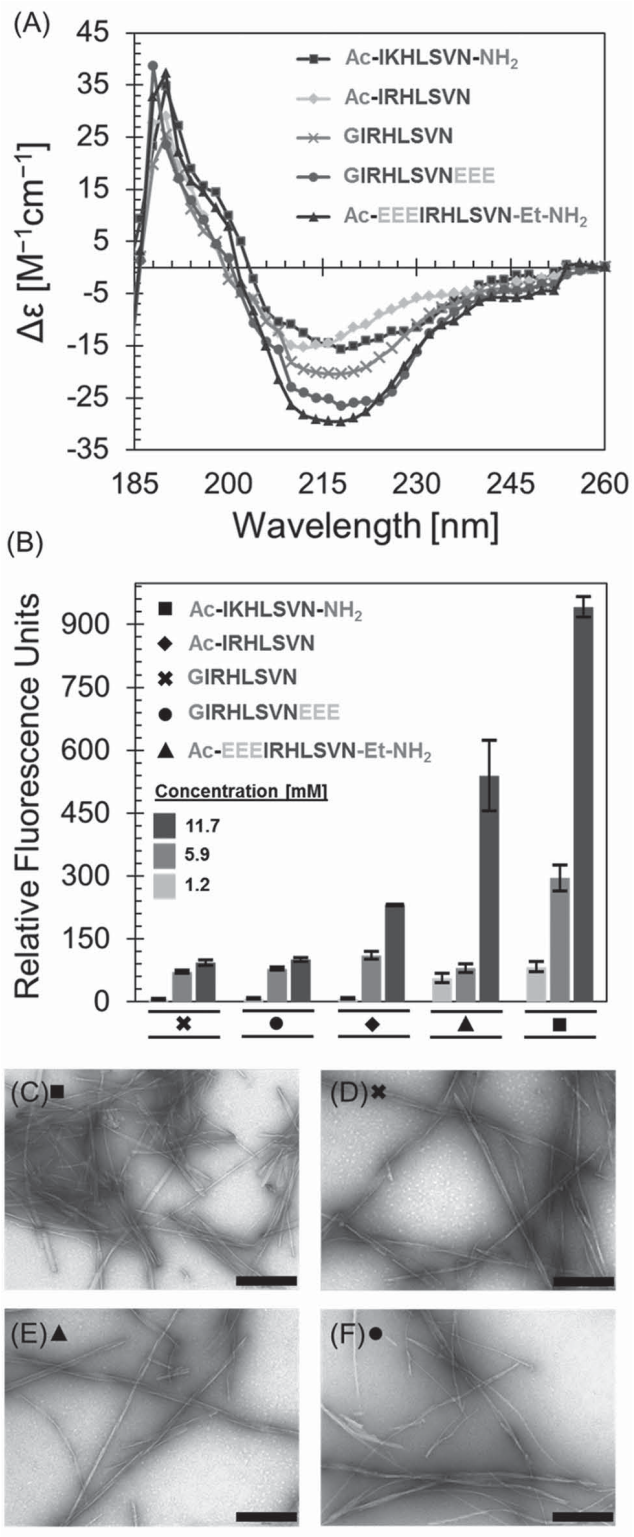

Figure 1. A) CD spectra of the native peptides for five relevant sequence variations (aqueous buffer solution, 0.1 mg mL^{-1} peptide concentration). B) Results of a thioflavin-T assay of the native peptides (24 h duration, at three peptide concentrations). Selected TEM images of the self-assembled native peptide nanofibers are shown for C) Ac-IKHLSVN-NH_2, D) GIRHLSVN, E) Ac-EEEIRHLSVN-ethyl-NH_2, and F) GIRHLSVNEEE (all scale bars = 200 nm).

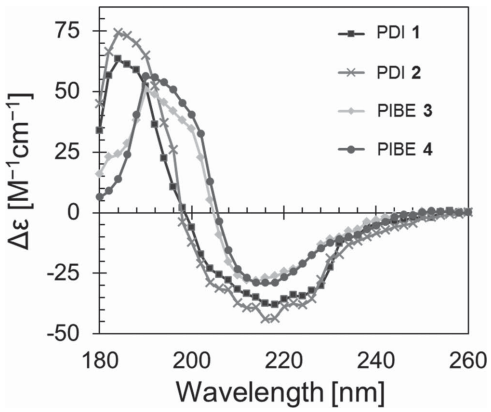

Figure 2. CD spectra along the 180–260 nm ultraviolet range, showing peptide substituent β-sheet formation in an aqueous solution of self-assembled PDIs **1**, **2** and PIBEs **3**, **4**.

Figure 1 confirmed that each of our modifications to the native sequence was innocent with respect to self-assembly; the lysine residue can be replaced with arginine, short linking units can be added, likewise for solublizing glutamic acid residues.

The CD signature of peptide β-sheet formation was also retained in the peptide–perylene imide conjugates. As shown in **Figure 2**, PDIs **1**, **2** and PIBEs **3**, **4** all displayed CD spectral profiles in the UV range consistent with that of β-sheet secondary structures. These spectra importantly demonstrate that the peptide substituents themselves are actively involved in the self-assembly of secondary structures for the overall peptide–perylene imide conjugates and are not just unnecessarily complex substituents exerting simple steric effects (or other bulk substituent influences) on the perylene core. Overlapping absorption and fluorescence from the perylene chromophore meant that the ThT assay could not be applied to these hybrid materials; however, the amide I bands of the IR spectra[39–42] for the PDIs and PIBEs (see Supporting Information Figures S27, S28, S29, and S30) were found to exhibit a band near 1630 cm^{-1} providing additional verification of β-sheet structure formation. Polarized IR spectroscopy could not be applied as a deeper probe of β-sheet structure because the TEM and atomic force microscopy (AFM) results (below) indicate that the relatively large optical IR beam will average over all orientations of fibers.

2.3. Optical Spectroscopy of Aggregates

Assembly of perylene moieties results in significant changes to visible optical absorption spectra. Since imide substituents do not directly affect the frontier molecular orbitals responsible for the visible electronic transition,[43] spectral changes can be used to understand how the substituents affect the relative orientations and electronic coupling between neighboring perylene monomers.[44,45] The UV–visible absorption spectra shown in **Figure 3** show that solutions of each of the peptide-substituted perylene imides exhibited clear signatures of aggregation and reveal important distinctions between each other.

Solutions of PDIs **1**, **2** in dimethysulfoxide (DMSO) (Figure 3A) both displayed a monomeric spectral profile with minimal differences between each other. Their monomeric

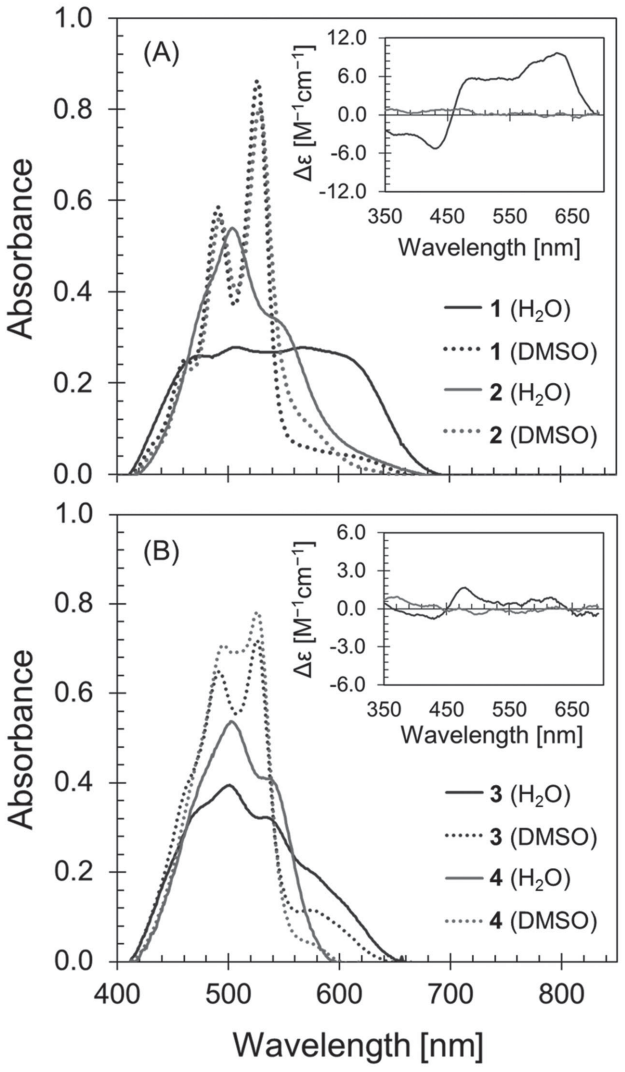

Figure 3. UV–vis spectra in DMSO and water with visible CD spectra of the aqueous solutions (insets) for A) PDIs **1**, **2** and B) PIBEs **3**, **4**.

nature was indicated by a band with a distinctive three-peak vibronic progression with ≈1400 cm^{-1} splitting and diminishing intensity for higher energy transitions. However, in aqueous solution, spectra of compounds **1** and **2** were dramatically different, indicating very different modes of monomer self-assembly. In water, PDI **1** displayed a very broad spectral profile, echoing traits of spectra reported for ordered liquid crystalline phases of PDI derivatives.[46–50] The suppression of vibronic structure, along with the enhanced low-energy absorption beyond 600 nm, suggests strong coupling between delocalized π-orbitals, which is a highly desirable property for electronic devices. Moreover, a Cotton effect observed in the visible region of the CD spectrum (inset, Figure 3A) indicated that the peptide directs assembly of the perylene monomers into ordered, chiral aggregates.[51,52]

PDI **2**—in which the peptide backbone orientation is reversed—gave a very different spectral profile than PDI **1** in water, in spite of their similar composition. The absorption spectrum of PDI **2** does not show the broadening to low energy found for PDI **1**, yet it still differs considerably from the monomer spectrum. In PDI **2**, the intensity of the 0–0 vibronic transition near 540 nm is diminished relative to the 0–1 transition near 500 nm. This intensity pattern is a signature of an H-aggregated system in which cofacially stacked perylene units are rotational displaced with minimal lateral displacement.[53] For strongly exciton-coupled H-aggregates, the 0–0 transition is dipole forbidden, while higher vibronic transitions gain intensity via symmetry breaking vibrational modes. Observing a weaker 0–0 transition relative to the 0–1 transition, as in this case, is expected in a weaker coupling regime and when there is a rotational offset between chromophores.[54] The aggregates formed by PDI **2**, however, did not show a Cotton effect in the visible region of the CD spectrum (inset, Figure 3A), indicating that the assembly of the perylene units did not produce a chirally ordered arrangement. The contrasting absorption spectra of PDIs **1** and **2** for the aqueous solutions show that coupling between neighboring electronic units can be impacted by the backbone orientation of the naturally derived β-sheet forming peptide.

In contrast to PDIs **1** and **2**, the spectral profiles of PIBEs **3** and **4** (Figure 3B) were mutually very similar. In DMSO, PIBEs **3**, **4** both exhibited vibronically structured spectral profiles consistent with predominantly monomeric species; however, the vibronic peak ratio and the presence of a feature near 580 nm suggested some extent of aggregation. Regardless, a distinctive transition to a more highly aggregated state was evident in the aqueous solutions of PIBEs **3**, **4**. Similar to PDI **2** (above), the spectra of PIBEs **3** and **4** in water both displayed traits consistent with H-aggregate formation, and Cotton effects were absent in the visible CD spectra (inset, Figure 3B). The band observed for PIBE **3**, however, expressed a shoulder feature between 580 and 660 nm, suggesting additional contributions from some other aggregate species with a band-like character similar to that seen for PDI **1**. The absorption spectrum of PIBE **4** was slightly red-shifted compared to PIBE **3**, and with a slightly different vibronic ratio; however, these differences were minimal relative to the comparison of PDIs **1** and **2**. Since the same peptides are compared in both pairs of hybrids, the spectral similarity of PIBEs **3** and **4** may be explained by greater orientational freedom of the perylene moieties with aggregating peptides on only one side. Conversely, the peptide β-sheets in the symmetrical structures of PDIs **1** and **2** appear to constrain the perylene moiety in a specific configuration, which is strongly π-stacked in the case of PDI **1**. Although beyond the scope of this investigation, the strong variation of optical and electronic coupling as a function of the peptide structure suggests these materials may also have promising nonlinear optical properties.

The reversed peptide backbones of PDIs **1** versus **2** suggested the possibility of blending the two materials to assemble them via antiparallel β-sheets that more closely mimic the natural protein system. Such an arrangement could be supported in alternating stacks of PDIs **1** and **2**, and may result in modified electronic properties for the central PDI core. However, equimolar binary mixtures of PDIs **1** and **2** were not found to produce any synergistic spectroscopic effects, rather the spectra could be explained by a statistical mixture of the two compounds (Supporting Information Figure S31). These results do not exclude the possibility of realizing an antiparallel

self-assembly motif, but they suggest that the assembly conditions may need to be optimized and the linker groups refined (length, conformational flexibility, etc.) in order to achieve the desired registry between neighboring molecules.

2.4. Nanostructure Formation

The aggregate species spectroscopically characterized in solution were confirmed, in most cases, to result from ordered nanofiber assemblies that were visualized by AFM and TEM. As shown in **Figure 4**A–C, PDI compounds **1**, **2** and PIBE **3** assembled into diffusive interlaced networks of narrow fibers. The notable exception was compound PIBE **4** (Figure 4D), which appeared to form only amorphous, plate-like accretions under the conditions tested. Extensive fibrillar formation was also seen for PDIs **1**, **2** via TEM, as shown in **Figure 5**. Out of the fiber-forming compounds, PDI **1** appeared to have a slight morphological distinction, presenting clusters of fiber networks with greater fiber density, length, and width. By AFM, the fiber segments formed by PDI **2** and PIBE **3** appeared to be roughly 100–200 nm in length, whereas the fibers formed by PDI **1** were longer, being roughly 200–300 nm long within the fiber clusters and exceeding a micrometer for isolated strands visible between the clusters. By both TEM and AFM, PDI **1** was clearly seen to form fibers of greater size than PDI **2**, with PDI **1** forming more ribbon-like structures in comparison to the thread-like assemblies of PDI **2** (Figure 5).

The morphological differences between compound pairs **1**, **2** and **3**, **4** (along with the spectroscopic distinctions noted previously) highlight the relevance of the mode of peptide sequence attachment toward self-assembly outcomes. Comparison of the morphologies observed via microscopy informed by the spectroscopic indications from solution suggested that PDI **1** provided larger, longer range nanostructures that were the most promising for field-effect device applications out of the four compounds studied.

2.5. OFET Fabrication and Performance

After examining the peptide-driven aggregation of each compound, biOFET devices were fabricated using them as the active semiconductor layer. As shown in **Figure 6**A, the devices were fabricated on highly doped silicon substrates (serving as the back gate) using a bottom-contact gold electrode channel configuration, with a spin-coated layer of polydimethylsiloxane (PDMS) acting as a dielectric layer. Flakes of the perylene imide active material were grown via slow solvent evaporation in small vials and transferred to span across an electrode channel on substrates with prepatterned electrodes applied onto a PDMS dielectric layer. Contact between the flakes and the gold electrodes was enhanced by the conductive silver paste. This approach was taken because the films were too brittle to survive mechanical contact with the shadow mask required for thermal evaporation of contacts. The PDMS layer also acted as an adhesive for the flakes on the device substrate. The brittle nature of the active material samples also made it very easy to break the devices by mechanical actions post deposition onto the PDMS films.

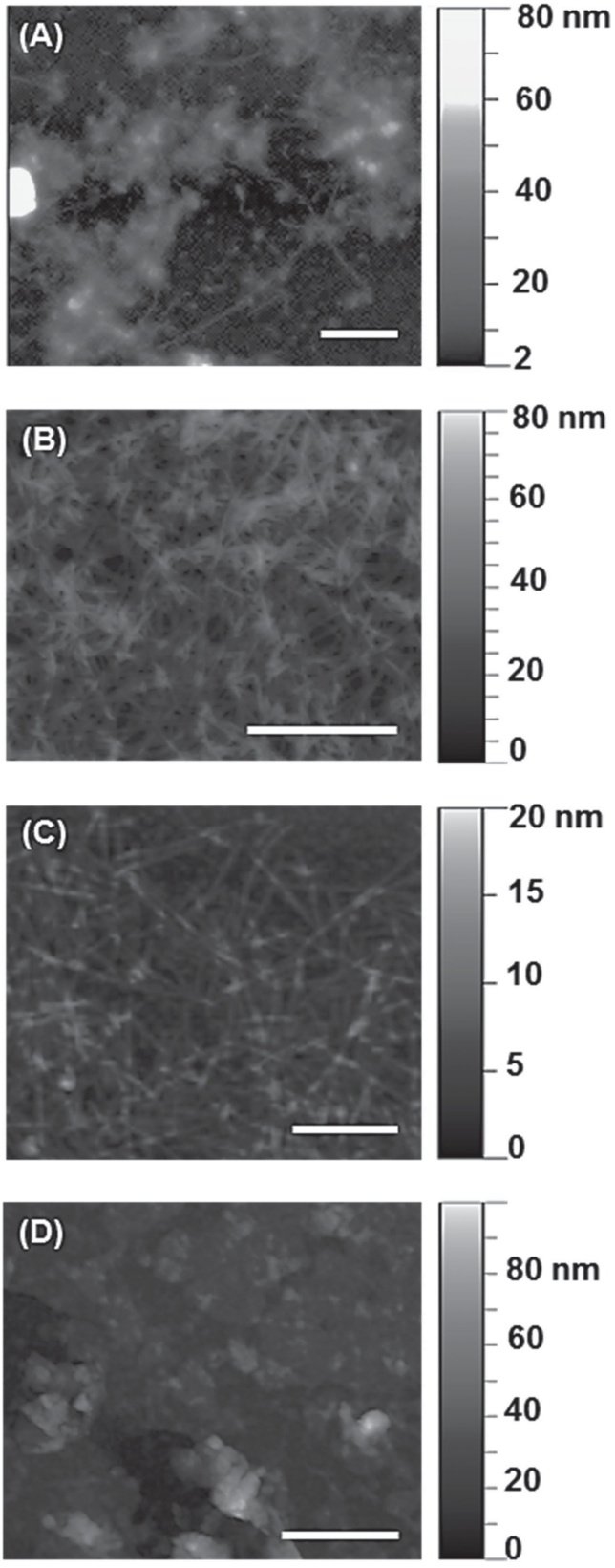

Figure 4. AFM images of dry nanofibers deposited on mica of A) PDI **1** (scale bar = 500 nm), B) PDI **2** (scale bar = 500 nm), C) PIBE **3** (scale bar = 25 nm), and D) PIBE **4** (scale bar = 500 nm).

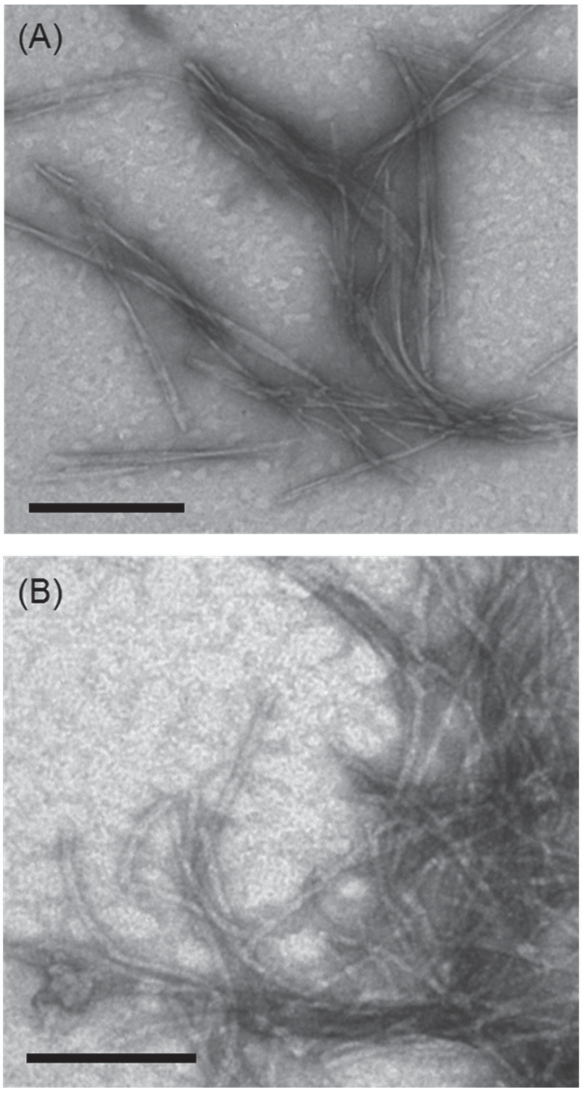

Figure 5. Negatively stained, dry TEM images of self-assembled nanofibers deposited on carbon-coated Formvar 200-mesh copper grids: A) PDI **1** (scale bar = 200 nm) and B) PDI **2** (scale bar = 100 nm).

Of the materials examined in this study, only PDI **1** yielded functioning devices, giving output and transfer characteristics as shown in Figure 6B,C. Although n-type semiconducting behavior was anticipated as being most probable for PDI **1** because of the high electron affinity of the perylene core and numerous examples of n-type behavior reported for perylene imide materials in the literature,[55] the output characteristics of PDI **1** (Figure 6B) are consistent with weak p-type behavior, yielding a decreasing current with increasing positive gate bias. Ongoing investigations of this unexpected behavior, for example surface dipole measurements, may reveal the role of the peptide and associated ions in modulating charge injection and transport in this material. Using these output curves to extract the ratio between the magnitude of the drain current (I_{DS}) at the highest and lowest gate voltage (I_{DS} taken at V_{DS} = 45 when V_G = ±50, the on/off ratio (I_{on}/I_{off}) for the device was evaluated to be 1.7. From the transfer plot

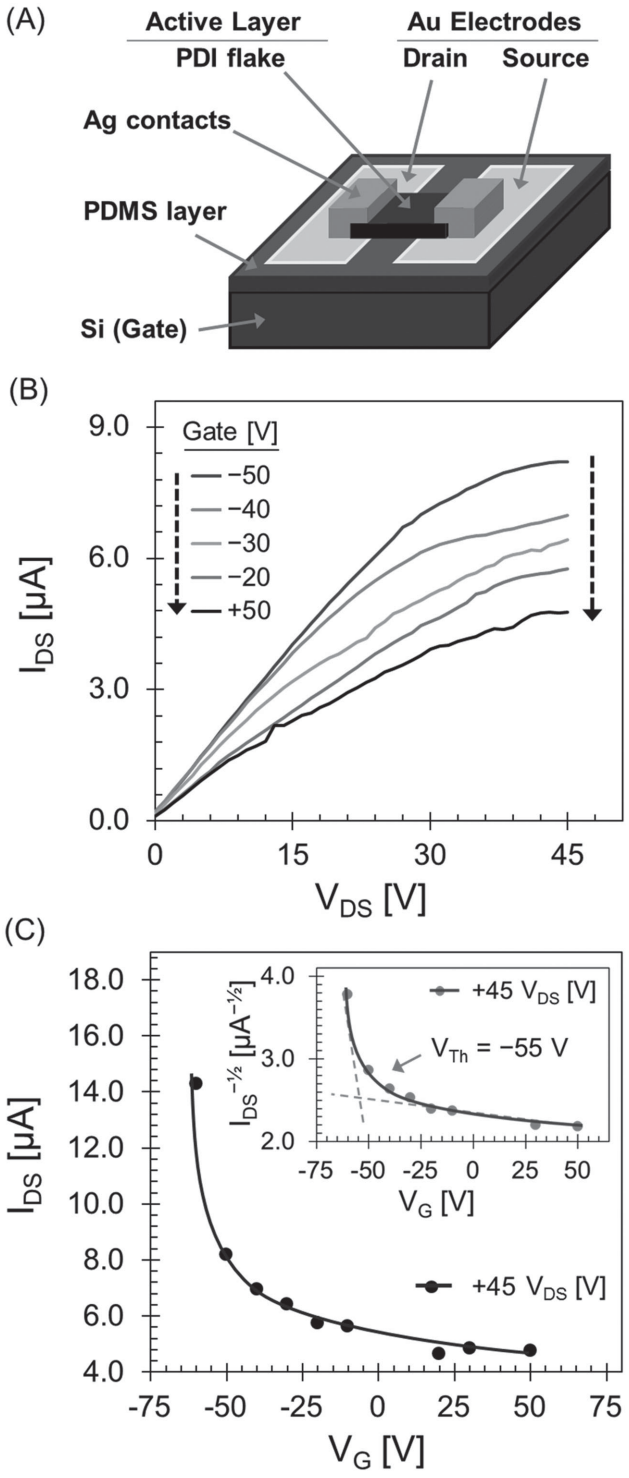

Figure 6. Device performance measurements of an organic field-effect transistor fabricated utilizing PDI **1** across a 40 μm channel. A) Device fabrication schematic; B) output characteristics; C) transfer characteristics with threshold voltage evaluation (inset).

in Figure 6C, the threshold voltage for the device was evaluated to occur near −55 V. It should be noted that the PDMS layer is on the order of 10 μm thick and therefore the field-dependent nature of the PDI **1** may be more apparent if a

thinner dielectric or a material with a higher dielectric constant is used. The field dependency was observed on several samples and the example shown in Figure 6 B,C is representative of the behavior and was observed, irrespective of the doping polarity of the underlying Si back gate. The poorly defined channel dimensions in this contact configuration prevented deeper analysis of the device response. However, the proof-of-concept demonstration provides the impetus to create next-generation materials that are compatible with the tightly controlled dimensions and interfaces desired in devices. As well as optimizing device performance, next-generation materials may enable deeper insights into the electronic behavior of this new class of bioelectronic material, particularly its interfaces with electrodes and dielectric layers.

3. Conclusion

We have created a new class of hybrid materials featuring organic semiconductors augmented with aggregating β-sheet peptide interfaces derived from natural Prx proteins. We confirmed that the peptides retain their β-sheet forming propensity when additional amino acids and linker units were added to manipulate their solubility and coupling with perylene imides. A series of perylene imides substituted with the same core peptide sequence (IRHLSVN) were synthesized to compare the effect of the number of peptide substituents and the directionality of their connectivity. Optical absorption and CD spectroscopy revealed distinct differences in the electronic coupling between neighboring perylene units imparted by the peptides, which was also manifest in different fiber morphologies. The bis-substituted material where the peptides were oriented in the N-to-C direction (away from the PDI) resulted in strong π-stacking and long-range order. These properties were exploited in the realization of a biOFET device with unexpected p-type behavior. The approach outlined highlights the opportunity to create hybrid functional materials with new properties by repurposing natural peptide sequences to encode their self-assembly. Next-generation materials may provide better performing devices, for example by replacing the perylene imide component with an organic semiconductor whose order is additionally influenced by its own hydrogen bonding interactions.

4. Experimental Section

Materials: Amino acid derivatives, synthetic resins, chemical reagents, and solvents were purchased in high purity from various commercial suppliers and used as received. Ac-IKHLSVN-NH_2 peptide was purchased from Mimotopes (Melbourne, Australia) with a purity of >95% (as an acetate salt). All other peptides were synthesized via standard Fmoc SPPS protocols. Synthesis of all peptide–perylene imide conjugates was accomplished via condensation of the terminal peptide amines (or amine linkers) with the desired perylene anhydride moiety. Full synthetic and characterization details (including nuclear magnetic resonance spectroscopy and mass spectrometry) for all compounds can be found in the Supporting Information.

AFM: AFM images were acquired using a Bruker MultiMode 8 with Nanoscope J controller. Samples were scanned in ScanAsyst mode using a ScanAsyst-Air tip (Silicon Nitride, 2–12 nm tip radius, $k = 0.4$ N m^{-1}). The sample environment was a Bruker stainless steel cantilever holder (MFMA), and all samples were imaged in air. Images were processed using Gwyddion 2.28 software. In a typical experiment, 1 mg of sample was briefly sonicated and gently heated into a pyridine/water mixture (9:1) yielding a red solution. An equimolar equivalent of glacial acetic was then added to neutralize the residual pyridine in solution. An aliquot (50 µL) of this solution was then spread onto a freshly cleaved mica substrate and left to dry for 24 h before imaging.

TEM: The peptide samples were pelleted by centrifuging at 10 000 rpm for 10 min. The pellet was then resuspended in 2.5% glutaraldehyde solution and stored overnight at 4 °C. Following overnight incubation, the peptide sample was repelleted and further suspended in water prior to grid preparation. (Note: The volume of water added was the same as that of the decanted supernatant to maintain the concentration.) Carbon-coated Formvar 200-mesh copper grids (ProSciTech, Australia) were deposited successively for 1 min each onto 15 µL drops of (i) aqueous peptide solutions, (ii) water (three times), and (iii) a 2% w/w uranyl acetate solution in water (as a negative stain). Filter paper was used to remove the excess liquid from the grids, which were then left to dry for a few hours before electron microscopy observations. The grids were examined with a FEI Morgagni 268D transmission electron microscope operating at 80 kV, with magnifications up to 180 000×. Micrographs were captured using an SIS/Olympus Megapixel III digital camera mounted above the phosphor screen.

UV–Vis Spectroscopy: UV–vis absorption spectra were collected on an Agilent 8463 UV–vis spectrometer using a 1.0 cm quartz cell. Micromolar solutions for spectroscopic analysis were prepared by diluting a 40 µL of a perylene imide stock solution into 5.0 mL of solvent. Stock solutions were prepared by dissolving 1.3–1.8 mg of compound into 1.0 mL of either trifluoroacetic acid (TFA) (for the PDIs) or 1:4 pyridine/water (for the PIBEs). PDI stock solutions were diluted into water, and PIBE stock solutions were diluted into 1 M HCl, producing spectroscopic solutions with residual acid to trigger compound self-assembly. Spectroscopic blanks were prepared analogously by diluting 40 µL of pristine stock solvent into 5.0 mL of the respective dilution solvent. All spectra were baseline corrected to remove effects attributed to scattering from aggregated particles.

CD Spectroscopy: Spectra were recorded at room temperature using a 1.0 cm quartz cell. Far UV CD spectra were collected with a Jasco J-815 spectrometer, and visible CD spectra were recorded on an Applied Photophysics Chirascan CD spectrometer. Solutions for analysis were prepared using the methods outlined for UV–vis spectroscopy. Solutions for analysis in the far UV were prepared from stock solutions dissolved in 0.1 M NaOH and made with an adjusted dilution factor.

ThT Fluorescence Binding Assays: Peptide samples were dissolved in an aqueous solution of ThT, such that the final concentrations in each sample were 25×10^{-6} M ThT and 1–10 mg mL^{-1} of peptide. The peptide solutions analyzed were prepared by diluting from aqueous stock solutions with concentrations of 20–30 mg mL^{-1}. Upon dilution, the resulting solutions to be analyzed were left to equilibrate at 4 °C for 24 h before recording fluorescence intensity. Fluorescence intensity was measured from 100 µL aliquots placed into sample well plates using a Molecular Devices SpectraMax M5 fluorimeter equipped with a plate reader. Samples were excited at 440 nm, and fluorescence intensity was recorded at 482 nm, using a 25×10^{-6} M ThT solution in water as a blank. The fluorescence intensity values reported resulted from the average of three recordings for each sample. For the samples analyzed, an additional turbidity assay was also performed as supporting evidence for the aggregation of the peptide sequences, showing the absorbance of the peptide solutions recorded at 600 nm (Supporting Information Figure S34).

Device Fabrication: biOFET devices were fabricated by integrating flakes of the hybrid peptide material as the active channel in a bottom contact, back gate device structure. Initially the device substrates were prepared by taking highly doped n-type silicon substrates (Silicon Quest International) and depositing a gold electrode onto the silicon to act as the back gate. P-type silicon substrates were also tested for a comparison. The top surfaces were then spin coated with PDMS (sylgard 184) at 6000 rpm for 60 s on highly doped (0.01–0.02 Ω cm)

n-type silicon substrates to provide the dual purpose of a gate dielectric, as well as being a soft and adhesive site for the peptide flakes. Gold electrodes (70 nm) with channel widths of 40 μm channel spacing were deposited via a precision Ossila OFET shadow mask using the Angstrom Engineering Nexdep evaporator. Flakes of the active materials were then mounted across the gold electrode channels using conductive silver paste (ethyl acetate paste solvent). All device measurements were conducted in air at room temperature.

Supporting Information

Supporting Information is available from the Wiley Online Library or from the author.

Acknowledgements

The UNSW contribution to this work was supported by the Australian Research Council under Linkage Grant [LP130100774], ARC Centre of Excellence [CE140100036], and Future Fellowship [FT120100101 to P.T]. The authors gratefully acknowledge Dr. Jeff Tallon and the Robinson Research Institute of Victoria University of Wellington for the use of their CD spectrometer, and the Biomedical Imaging Facility (BMIF-MWAC) at UNSW for access to AFM. They also thank Ian Vorster and Dr. Rob Keyzers for assistance with mass spectrometry and NMR spectroscopy, Cameron Wood for facilitating initial device testing trials, and Shyamal Prasad for assisting in the spectral data-fitting analyses.

Received: June 2, 2015
Revised: July 8, 2015
Published online: August 4, 2015

[1] S. Zhang, *Biotechnol. Adv.* **2002**, *20*, 321.
[2] S. H. Waterhouse, J. A. Gerrard, *Aust. J. Chem.* **2004**, *57*, 519.
[3] R. G. Ellis-Behnke, Y.-X. Liang, S.-W. You, D. K. C. Tay, S. Zhang, K.-F. So, G. E. Schneider, *Proc. Natl. Acad. Sci. USA* **2006**, *103*, 5054.
[4] A. J. Phillips, J. Littlejohn, N. A. Yewdall, T. Zhu, C. Valéry, F. G. Pearce, A. K. Mitra, M. Radjainia, J. A. Gerrard, *Biomacromolecules* **2014**, *15*, 1871.
[5] P. A. Karplus, A. Hall, in *Peroxiredoxin Systems* (Eds: L. Flohé, J. R. Harris), Springer Science and Business Media Inc., New York, NY, USA **2007**, pp. 41–60.
[6] F. Angelucci, F. Saccoccia, M. Ardini, G. Boumis, M. Brunori, L. Di Leandro, R. Ippoliti, A. E. Miele, G. Natoli, S. Scotti, A. Bellelli, *J. Mol. Biol.* **2013**, *425*, 4556.
[7] H. Kato, M. Asanoi, T. Nakazawa, K. Maruyama, *Zool. Sci.* **1985**, *2*, 485.
[8] J. R. Harris, E. Schröder, M. N. Isupov, D. Scheffler, P. Kristensen, J. A. Littlechild, A. A. Vagin, U. Meissner, *Biochim. Biophys. Acta* **2001**, *1547*, 221.
[9] H. H. Jang, K. O. Lee, Y. H. Chi, B. G. Jung, S. K. Park, J. H. Park, J. R. Lee, S. S. Lee, J. C. Moon, J. W. Yun, Y. O. Choi, W. Y. Kim, J. S. Kang, G.-W. Cheong, D.-J. Yun, S. G. Rhee, M. J. Cho, S. Y. Lee, *Cell* **2015**, *117*, 625.
[10] U. Meissner, E. Schröder, D. Scheffler, A. G. Martin, J. R. Harris, *Micron* **2007**, *38*, 29.
[11] C. Valéry, R. Pandey, J. A. Gerrard, *Chem. Commun.* **2013**, *49*, 2825.
[12] I. M. A. Nooren, J. M. Thornton, *J. Mol. Biol.* **2003**, *325*, 991.
[13] S. Dey, A. Pal, P. Chakrabarti, J. Janin, *J. Mol. Biol.* **2010**, *398*, 146.
[14] M. Irimia-Vladu, *Chem. Soc. Rev.* **2014**, *43*, 588.
[15] T. Cipriano, G. Knotts, A. Laudari, R. C. Bianchi, W. A. Alves, S. Guha, *ACS Appl. Mater. Interfaces* **2014**, *6*, 21408.
[16] J.-W. Chang, C.-G. Wang, C.-Y. Huang, T.-D. Tsai, T.-F. Guo, T.-C. Wen, *Adv. Mater.* **2011**, *23*, 4077.
[17] T. Singh, N. Sariciftci, J. Grote, in *Organic Electronics SE-6*, Advances in Polymer Science, Vol. 223, Springer, Berlin–Heidelberg, Germany **2010** pp. 73–112.
[18] S. T. Yau, G. Qian, *Appl. Phys. Lett.* **2005**, *86*, 1.
[19] M. Mizrahi, A. Zakrassov, J. Lerner-Yardeni, N. Ashkenasy, *Nanoscale* **2012**, *4*, 518.
[20] C. Liao, F. Yan, *Polym. Rev.* **2013**, *53*, 352.
[21] Y.-W. Kwon, C. H. Lee, D.-H. Choi, J.-I. Jin, *J. Mater. Chem.* **2009**, *19*, 1353.
[22] M. B. Avinash, T. Govindaraju, *Nanoscale* **2011**, *3*, 2536.
[23] Y. Sun, C. He, K. Sun, Y. Li, H. Dong, Z. Wang, Z. Li, *Langmuir* **2011**, *27*, 11364.
[24] H. Shao, J. R. Parquette, *Chem. Commun.* **2010**, *46*, 4285.
[25] M. O. Guler, R. C. Claussen, S. I. Stupp, *J. Mater. Chem.* **2005**, *15*, 4507.
[26] R. Matmour, I. De Cat, S. J. George, W. Adriaens, P. Leclère, P. H. H. Bomans, N. A. J. M. Sommerdijk, J. C. Gielen, P. C. M. Christianen, J. T. Heldens, J. C. M. van Hest, D. W. P. M. Löwik, S. De Feyter, E. W. Meijer, A. P. H. J. Schenning, *J. Am. Chem. Soc.* **2008**, *130*, 14576.
[27] J. K. Gallaher, E. J. Aitken, R. A. Keyzers, J. M. Hodgkiss, *Chem. Commun.* **2012**, *48*, 7961.
[28] G. L. Eakins, J. K. Gallaher, R. A. Keyzers, A. Falber, J. E. A. Webb, A. Laos, Y. Tidhar, H. Weissman, B. Rybtchinski, P. Thordarson, J. M. Hodgkiss, *J. Phys. Chem. B* **2014**, *118*, 8642.
[29] R. J. Kumar, J. M. MacDonald, T. B. Singh, L. J. Waddington, A. B. Holmes, *J. Am. Chem. Soc.* **2011**, *133*, 8564.
[30] I. Coin, M. Beyermann, M. Bienert, *Nat. Protoc.* **2007**, *2*, 3247.
[31] A. Wicklein, A. Lang, M. Muth, M. Thelakkat, *J. Am. Chem. Soc.* **2009**, *131*, 14442.
[32] S. Henikoff, J. G. Henikoff, *Proc. Natl. Acad. Sci. USA* **1992**, *89*, 10915.
[33] M. J. Betts, R. B. Russell, in *Bioinformatics for Geneticists: A Bioinformatics Primer for the Analysis of Genetic Data*, (Eds: M. R. Barnes, I. C. Gray), John wiley and Sons Ltd, Chichester, UK **2003**, p. 311.
[34] J. D. Hartgerink, E. Beniash, S. I. Stupp, *Proc. Natl. Acad. Sci. USA* **2002**, *99*, 5133.
[35] A. Dehsorkhi, V. Castelletto, I. W. Hamley, *J. Pept. Sci.* **2014**, *20*, 453.
[36] S. M. Kelly, T. J. Jess, N. C. Price, *Biochim. Biophys. Acta* **2005**, *1751*, 119.
[37] M. Biancalana, S. Koide, *Biochim. Biophys. Acta* **2010**, *1804*, 1405.
[38] R. Khurana, C. Coleman, C. Ionescu-Zanetti, S. A. Carter, V. Krishna, R. K. Grover, R. Roy, S. Singh, *J. Struct. Biol.* **2005**, *151*, 229.
[39] J. L. Arrondo, F. M. Goñi, *Prog. Biophys. Mol. Biol.* **1999**, *72*, 367.
[40] D. M. Byler, H. Susi, *Biopolymers* **1986**, *25*, 469.
[41] M. Bloemendal, W. C. Johnson, *Pharm. Biotechnol.* **1995**, *7*, 65.
[42] W. K. Surewicz, H. H. Mantsch, G. L. Stahl, R. M. Epand, *Proc. Natl. Acad. Sci. USA* **1987**, *84*, 7028.
[43] F. Würthner, *Chem. Commun.* **2004**, 1564.
[44] S. Ghosh, X. Q. Li, V. Stepanenko, F. Würthner, *Chem. Eur. J.* **2008**, *14*, 11343.
[45] J. Seibt, P. Marquetand, V. Engel, Z. Chen, V. Dehm, F. Würthner, *Chem. Phys.* **2006**, *328*, 354.
[46] S. G. Liu, G. Sui, R. A. Cormier, R. M. Leblanc, B. A. Gregg, *J. Phys. Chem. B* **2002**, *106*, 1307.

[47] B. Gao, D. Xia, L. Zhang, Q. Bai, L. Bai, T. Yang, X. Ba, *J. Mater. Chem.* **2011**, *21*, 15975.
[48] T. Zhang, D. Sun, X. Ren, L. Liu, G. Wen, Z. Ren, H. Li, S. Yan, *Soft Matter* **2013**, *9*, 10739.
[49] N. Mizoshita, T. Tani, S. Inagaki, *Adv. Funct. Mater.* **2011**, *21*, 3291.
[50] C. W. Struijk, A. B. Sieval, J. E. J. Dakhorst, M. Van Dijk, R. B. M. Koehorst, H. Donker, T. J. Schaafsma, S. J. Picken, A. M. Van De Craats, J. M. Warman, H. Zuilhof, E. J. R. Sudhlter, *J. Am. Chem. Soc.* **2000**, *122*, 11057.
[51] D. Franke, M. Vos, M. Antonietti, N. A. J. M. Sommerdijk, C. F. J. Faul, *Chem. Mater.* **2006**, *18*, 1839.
[52] R. Marty, R. Szilluweit, A. Sánchez-Ferrer, S. Bolisetty, J. Adamcik, R. Mezzenga, E.-C. Spitzner, M. Feifer, S. N. Steinmann, C. Corminboeuf, H. Frauenrath, *ACS Nano* **2013**, *7*, 8498.
[53] Z. Chen, V. Stepanenko, V. Dehm, P. Prins, L. D. A. Siebbeles, J. Seibt, P. Marquetand, V. Engel, F. Wuerthner, *Chem. Eur. J.* **2007**, *13*, 436.
[54] F. C. Spano, *Acc. Chem. Res.* **2010**, *43*, 429.
[55] Y. Zhao, Y. Guo, Y. Liu, *Adv. Mater.* **2013**, *25*, 5372.